

The optomechanical instability in the quantum regime

Max Ludwig, Björn Kubala, and Florian Marquardt

October 22, 2018

Department für Physik, Arnold Sommerfeld Center for Theoretical Physics,
and Center for NanoScience, Ludwig-Maximilians-Universität München, There-
sienstr. 37, D-80333 München, Germany

Abstract

We consider a generic optomechanical system, consisting of a driven optical cavity and a movable mirror attached to a cantilever. Systems of this kind (and analogues) have been realized in many recent experiments. It is well known that those systems can exhibit an instability towards a regime where the cantilever settles into self-sustained oscillations. In this paper, we briefly review the classical theory of the optomechanical instability, and then discuss the features arising in the quantum regime. We solve numerically a full quantum master equation for the coupled system, and use it to analyze the photon number, the cantilever's mechanical energy, the phonon probability distribution and the mechanical Wigner density, as a function of experimentally accessible control parameters. We observe and discuss the quantum-to-classical transition as a function of a suitable dimensionless quantum parameter.

1 Introduction

Light interacting with matter can not only be scattered, absorbed and emitted by individual atoms, but it can also lead to mechanical effects. The radiation pressure of light was first directly observed in the seminal experiments of Nichols and Hull in 1901 and, independently, by Lebedev, where it exerted a torque on a pair of glass mirrors inside an evacuated chamber. Radiation pressure can also deflect the tail of comets (as first hypothesized by Johannes Kepler), or change the path of asteroids. The mechanical effects of light become most pronounced in an optical cavity where the light intensity is resonantly enhanced, and where one of the end-mirrors is made movable, e.g., by being attached to a cantilever (Fig. 1). The pioneering theoretical and experimental works in this domain are due to Braginsky [1, 2]. In the 80s, strong effects were observed by the MPQ group of H. Walther in a setup using a macroscopic mirror [3]. More recently, the trend has been to exploit the tools of microfabrication to fabricate small

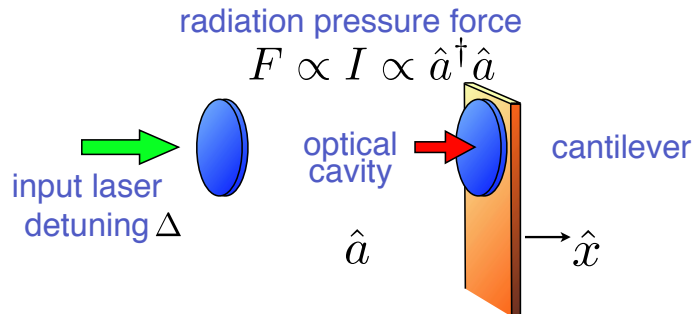


Figure 1: The basic optomechanical setup.

cantilevers, nanobeams or other mechanical elements that can be affected by light. The small masses, high mechanical quality factors and (in some of the experiments) high optical finesse in these setups increase the optomechanical effects. Several recent experiments have demonstrated optomechanical cooling [4, 5, 6, 7, 8, 9, 10, 11], where the time-delayed light-induced forces lead to additional damping. Such a scheme may ultimately be employed to cool down to the ground-state of mechanical motion [12, 13].

On the other hand, the light-induced forces can also lead to a negative contribution to the overall damping rate. At first, this increases the mechanical Q of the mechanical degree of freedom (hereafter simply referred to as the cantilever), and can thus serve to amplify the response to any noise source acting on the cantilever. Once the overall “damping rate” becomes negative, which can happen simply by increasing the light power entering the cavity, we no longer have damping but instead an instability [14, 15, 16, 17]. The cantilever starts to oscillate at its eigenfrequency, with an amplitude that at first increases exponentially and then saturates to a steady-state value. These self-induced oscillations have by now been observed in several experiments [18, 19, 20, 21]. Theoretical studies predict an intricate attractor diagram [17], which can display multiple stable attractors (i.e. possible oscillation amplitudes) for a given set of fixed external parameters. This attractor diagram has recently been observed and studied systematically in a low-finesse setup dominated by bolometric forces, which exhibited the unexpected feature of simultaneous excitation of several mechanical modes [21].

Similar physics has by now been observed in a variety of other systems which do not contain any optical elements. This includes driven LC circuits coupled to cantilevers [22], single-electron transistors and microwave cavities coupled to nanobeams [23, 24, 25, 26, 27, 28, 29, 30], as well as clouds of cold atoms in an optical lattice inside a cavity [31, 32].

The common characteristic of all of these systems is that they contain some driven resonant quantum system (optical or microwave cavity, LC circuit, superconducting single-electron transistor), whose resonance frequency depends

on the motion of a mechanical degree of freedom (cantilever, nanobeam, deformation of a microtoroidal optical resonator, collective coordinate of a cloud of atoms). Their Hamiltonian thus is typically of the form

$$\hat{H} = \hbar\omega_R(\hat{x})\hat{a}^\dagger\hat{a} + \hbar\omega_M\hat{c}^\dagger\hat{c} + \dots, \quad (1)$$

where \hat{a} is the photon annihilation operator for the driven resonator, whose frequency depends on the coordinate $\hat{x} = x_{\text{ZPF}}(\hat{c} + \hat{c}^\dagger)$ of the mechanical oscillator with frequency ω_M . Usually, it is possible to a very good approximation to expand ω_R to linear order in \hat{x} , which is the case we will assume in the following. The additional terms not displayed in Eq. (1) then describe the driving, as well as the damping and the fluctuation terms coupling to both oscillators (see below).

Cooling to the mechanical ground-state will generate the opportunity to observe a variety of quantum effects in such systems, including “cat” states [33], entanglement [34, 35] and Fock state detection [11, 36]. For a recent review of optomechanical systems, see [37], and [38] for the quantum noise approach to cooling.

One question that may be asked about the quantum regime of these devices, that is now being approached experimentally, is how the instability discussed above changes due to quantum effects. We will answer this question partially in the present paper. We note that there have recently been some discussions of the quantum dynamics for the related instability in electronic systems in the literature [27, 28, 29, 39]. The most important dimensionless parameter entering our analysis will be the “quantum parameter”

$$\zeta \equiv \frac{x_{\text{ZPF}}}{x_{\text{FWHM}}}, \quad (2)$$

which denotes the ratio between the mechanical zero-point fluctuation amplitude (a quantum parameter, $\propto \sqrt{\hbar}$) and the width of the optical resonance (a classical quantity), measured in terms of displacement. After some rearrangement, one can see that this is essentially the “granularity” parameter employed in the discussion of the cold-atom experiment [32]. There, it was introduced by considering the total momentum kick a single photon would impart to the mechanical element, as it is reflected multiple times before leaving the cavity. The granularity parameter then would be derived from the ratio of this kick to the mechanical momentum ground-state uncertainty.

Increasing the quantum parameter ζ will enhance quantum effects on the motion of the cantilever. These include the effects of the photon shot noise, as well as the mechanical zero-point fluctuations. The purpose of the present paper is to discuss these features in their dependence on ζ . We note that ζ is rather small in the current optomechanical experiments (reaching up to about $\zeta \sim 10^{-3}$ in [9]). However, given the large variety of analogous systems that are now being considered, we feel that it is justified to illustrate some of the salient features of the “quantum-to-classical crossover” by also analysing the regime $\zeta \sim 1$.

The remainder of this paper is organized as follows: We will first introduce the model Hamiltonian, and, in particular, discuss the full set of dimensionless parameters that are needed in our analysis. We then review the classical regime of self-induced oscillations. In particular, we will discuss the attractor diagram for the “resolved sideband regime” $\omega_M \gg \kappa$, which has not been discussed before in this context. This regime is currently of considerable interest, as it is crucial for ground-state cooling [12, 13], and $\omega_M/\kappa \sim 20$ has recently been realized experimentally [40]. Then we will turn to the full quantum model, that is first being discussed in terms of the rate equations that can yield the behaviour below the instability threshold. Afterwards, the full-blown quantum dynamics of self-induced oscillations will be analyzed using a master equation approach applied to the coupled system consisting of optical mode and cantilever. We will illustrate how the average mechanical energy, as a function of laser detuning, approaches the known classical result when the quantum parameter is sent to zero. In our present analysis, we focus on the steady-state and also assume a thermal bath temperature of $T = 0$. In real optomechanical experiments, one would presumably first cool down using the light field and then observe the onset of nonlinear dynamics as the detuning is varied. Investigation of these effects would entail studying the complete nonequilibrium time-evolution.

2 Model and parameters

In this section we present the Hamiltonian of the coupled cavity-cantilever system. A reduced set of dimensionless parameters determining the dynamics of the coupled system is identified. In particular, we introduce a quantum parameter, which is absent in descriptions of the classical dynamics [17, 21] and governs the crossover from classical to quantum behavior of the coupled dynamics of cavity and cantilever.

2.1 Hamiltonian

To describe a system of a mechanical cantilever coupled to a driven cavity, we consider the Hamiltonian

$$\hat{H} = \hbar(-\Delta - g(\hat{c} + \hat{c}^\dagger))\hat{a}^\dagger\hat{a} + \hbar\omega_M\hat{c}^\dagger\hat{c} + \hbar\alpha_L(\hat{a} + \hat{a}^\dagger) + \hat{H}_\kappa + \hat{H}_\Gamma, \quad (3)$$

which is written in the rotating frame of the driving laser field of frequency ω_L , with an amplitude set by α_L . The laser is detuned by $\Delta = \omega_L - \omega_{\text{cav}}$ with respect to the optical cavity mode, described by photon annihilation and creation operators \hat{a} and \hat{a}^\dagger , and a photon number $\hat{n}_{\text{cav}} = \hat{a}^\dagger\hat{a}$. The cantilever (or, in general, mechanical element) of frequency ω_M and mass m has a phonon number $\hat{n}_M = \hat{c}^\dagger\hat{c}$, and its displacement is given as $\hat{x} = x_{\text{ZPF}}(\hat{c} + \hat{c}^\dagger)$, with the ground state position uncertainty (mechanical zero-point fluctuations) $x_{\text{ZPF}} = \sqrt{\hbar/(2m\omega_M)}$. The optomechanical coupling, between the optical field and the mechanical displacement, is characterized by the parameter g . In the simplest

case, with a movable, fully reflecting mirror at one end of an optical cavity, we have $g = \omega_{\text{cav}} x_{\text{ZPF}}/L$, and thus $g(\hat{c} + \hat{c}^\dagger) = \omega_{\text{cav}} \hat{x}/L$, with a radiation pressure force equal to $\hat{F}_{\text{rad}} = \hat{a}^\dagger \hat{a} \hbar g/x_{\text{ZPF}}$. The decay of a photon and the mechanical damping of the cantilever are captured by \hat{H}_κ and \hat{H}_{Γ_M} , respectively. They describe coupling to a bath leading to a cavity damping rate κ and mechanical damping Γ_M . Note that each of the parameters Δ , g , ω_M , α_L has the dimension of a frequency.

2.2 Reduction to a set of dimensionless and independent parameters

We now identify the dimensionless parameters the system dynamics depends on. Expressed in terms of the mechanical oscillator frequency ω_M , the parameters describing the classical system are

$$\begin{aligned}
\text{mechanical damping} & : \Gamma_M/\omega_M \\
\text{cavity decay} & : \kappa/\omega_M \\
\text{detuning} & : \Delta/\omega_M \\
\text{driving strength} & : \mathcal{P} = 8|\alpha_L|^2 g^2/\omega_M^4 = \omega_{\text{cav}} \kappa^2 E_{\text{max}}^{\text{cav}}/(\omega_M^5 m L^2).
\end{aligned}$$

Here $E_{\text{max}}^{\text{cav}}$ is the light energy circulating inside the cavity when the laser is in resonance with the optical mode. The quantum mechanical nature of the system is described by the ‘‘quantum parameter’’ ζ , comparing the magnitude of the cantilever’s zero-point fluctuations, x_{ZPF} , with the full width at half maximum (FWHM) of the cavity (translated into a cantilever displacement x_{FWHM})

$$\text{quantum parameter} : \zeta = \frac{x_{\text{ZPF}}}{x_{\text{FWHM}}} = \frac{g}{\kappa}.$$

The resonance width of the cavity can be expressed as $x_{\text{FWHM}} = \kappa L/\omega_{\text{cav}}$, where L is the cavity’s length. The quantum parameter ζ vanishes in the classical limit $\hbar \rightarrow 0$, as the zero-point fluctuations x_{ZPF} of the cantilever go to zero. The magnitude of ζ determines the effect of quantum fluctuations on the dynamics of the coupled cavity-cantilever system.

In later parts of this paper we will discuss the motion of the mechanical cantilever due to the driving of the cavity, both in a classical and a quantum mechanical picture. Such motion can be characterized by its energy E_M , which in the classical case directly follows from the oscillation amplitude A of the cantilever: $E_{M,\text{cl}} = \frac{1}{2} m \omega_M^2 A^2$. In a quantum mechanical treatment, the energy is obtained from the expectation value of the occupation number of the oscillator: $E_{M,\text{qm}} = \hbar \omega_M \langle \hat{n}_M \rangle$, where we exclude the zero-point energy. The dimensionless ratio of the cantilever energy E_M to a characteristic classical energy scale of the system is then easily compared for the two approaches. To set this characteristic energy scale, we take the energy $E_0 = \frac{1}{2} m \omega_M^2 x_{\text{FWHM}}^2$ associated with an oscillation amplitude x_{FWHM} of the mechanical cantilever which moves the cavity just out of its resonance. Note that $E_M/E_0 = (A/x_{\text{FWHM}})^2$ in the classical case, and $E_M/E_0 = 4\zeta^2 \langle \hat{n}_M \rangle$ in the quantum version.

3 Dynamics of the system

In this section, we will first briefly recapitulate the results of a classical treatment of the optomechanical system [17, 21]. We will concentrate on the regime of blue-detuned excitation of the cavity, where the cantilever motion is amplified and self-induced oscillations can occur. Amplification behaviour of the coupled system (away from the regime of self-induced oscillations) can be understood within a simple rate equation approach, which captures the effect of photon shot noise leading to fluctuations of the radiation pressure force acting on the cantilever [12]. The full quantum mechanical treatment, employing the numerical solution of a quantum master equation, can describe the crossover from heating/amplification to classical self-induced oscillations of the coupled system, where the quantum parameter $\zeta = x_{\text{ZPF}}/x_{\text{FWHM}}$ governs the quantum-to-classical transition.

3.1 Classical solution

Heisenberg equations of motion for the cavity operator \hat{a} and the cantilever position operator \hat{x} can easily be derived from the Hamiltonian, Eq. 3. To investigate the purely classical dynamics of the coupled cavity-cantilever system, we replace the operator $\hat{a}(t)$ by the complex light amplitude $\alpha(t)$ and the position operator of the cantilever \hat{x} by its classical counterpart. We thus arrive at:

$$\dot{\alpha} = [i(\Delta + g\frac{x}{x_{\text{ZPF}}}) - \frac{\kappa}{2}] \alpha - i\alpha_L \quad (4)$$

$$\ddot{x} = -\omega_M^2 x + \frac{\hbar g}{m x_{\text{ZPF}}} |\alpha|^2 - \Gamma_M \dot{x}. \quad (5)$$

Here fluctuations (both the photon shot noise as well as intrinsic mechanical thermal fluctuations) have been neglected, to obtain the purely deterministic classical solution. The variables t , x and α can be rescaled [17] as $\tilde{t} = \omega_M t$; $\tilde{\alpha} = i\alpha\omega_M/(2\alpha_L)$; $\tilde{x} = gx/(\omega_M x_{\text{ZPF}})$, so that the coupled equations of motion contain only the dimensionless parameters \mathcal{P} , Δ/ω_M , κ/ω_M , and Γ_M/ω_M :

$$\begin{aligned} \frac{d\tilde{\alpha}}{d\tilde{t}} &= [i(\frac{\Delta}{\omega_M} + \tilde{x}) - \frac{1}{2} \frac{\kappa}{\omega_M}] \tilde{\alpha} + \frac{1}{2} \\ \frac{d^2\tilde{x}}{d\tilde{t}^2} &= -\tilde{x} + \mathcal{P} |\tilde{\alpha}|^2 - \frac{\Gamma_M}{\omega_M} \frac{d\tilde{x}}{d\tilde{t}}. \end{aligned}$$

Crucially, the quantum parameter ζ cannot and does not feature in these equations.

Apart from a static solution $x(t) \equiv \text{const}$, this system of coupled differential equations can show self-induced oscillations. In such solutions, the cantilever conducts an approximately sinusoidal oscillation at its unperturbed frequency, $x(t) \approx \bar{x} + A \cos(\omega_M t)$. The radiation pressure affects the cantilever motion

rather weakly, so that the oscillation amplitude A varies only slowly and can be taken as constant during one oscillation period. The light amplitude then shows the dynamics of a damped, driven oscillator, which is swept through its resonance, see Eq. (4); an exact solution for the light amplitude $\alpha(t)$ can be given as a Fourier series containing harmonics of the cantilever frequency ω_M [17]:

$$|\tilde{\alpha}(\tilde{t})| = \left| \sum_n \tilde{\alpha}_n e^{in\tilde{t}} \right|, \quad (6)$$

with

$$\tilde{\alpha}_n = \frac{1}{2} \frac{J_n(-\tilde{A})}{in + \kappa/(2\omega_M) - i(\tilde{x} + \Delta/\omega_M)}. \quad (7)$$

The dependence of oscillation amplitude, A , and average cantilever position, \bar{x} , on the dimensionless system parameters can be found by two balance conditions: Firstly, the total force on the cantilever has to vanish on average, and, secondly, the power input into the mechanical oscillator by the radiation pressure on average has to equal the friction loss.

The force balance condition determines the average position of the oscillator, yielding an implicit equation for \bar{x} ,

$$\langle \ddot{x} \rangle \equiv 0 \quad \Leftrightarrow \quad m\omega_M^2 \bar{x} = \langle F_{\text{rad}} \rangle = \frac{\hbar g}{m x_{\text{ZPF}}} \langle |\alpha(t)|^2 \rangle, \quad (8)$$

where the average radiation force, $\langle F_{\text{rad}} \rangle$ is a function of the parameters \bar{x} and A .

The balance between the mechanical power gain due to the light-induced force, $P_{\text{rad}} = \langle F_{\text{rad}} \dot{x} \rangle$, and the frictional loss $P_{\text{fric}} = \Gamma_M \langle \dot{x}^2 \rangle$ follows from

$$\langle \dot{x} \ddot{x} \rangle \equiv 0 \quad \Leftrightarrow \quad \langle F_{\text{rad}} \dot{x} \rangle = \Gamma_M \langle \dot{x}^2 \rangle. \quad (9)$$

For each value of the oscillation amplitude A we can now plot the ratio between radiation power input and friction loss, $P_{\text{rad}}/P_{\text{fric}} = \langle F_{\text{rad}} \dot{x} \rangle / (\Gamma_M \langle \dot{x}^2 \rangle)$, after eliminating \bar{x} using Eq. 8. This is shown in Fig. 2. Power balance is fulfilled if this ratio is one, corresponding to the contour line $P_{\text{rad}}/P_{\text{fric}} = 1$. If the power input into the cantilever by radiation pressure is larger than frictional losses (i.e., for a ratio larger than one), the amplitude of oscillations will increase, otherwise it will decrease. Stable solutions (dynamical attractors) are therefore given by that part of the contour line where the ratio decreases with increasing oscillation amplitude (energy), as shown in Fig. 2.

Changing the (dimensionless) mechanical damping rate Γ_M/ω_M will scale the plot in Fig. 2 along the vertical axis, so that the horizontal cut at one yields a different contour line of stable solutions [a changed input power \mathcal{P} gives a similar scaling, but leads to further changes in the solution, as \mathcal{P} also enters the force balance condition, Eq. (8)]. Decreasing mechanical damping or increasing the

power input will increase the plot height in Fig. 2, so that the amplitude/energy of oscillation of the stable solution increases.

While the surface or contour plots in Fig. 2 allow a discussion of general features of the self-induced oscillations, such as the multistabilities discussed in Ref. [17], a slightly different representation of the classical solution is more amenable to an easier understanding of the particular dynamics of the system for a certain set of fixed system parameters. Figure 3 shows the cantilever energy $E_{M,\text{cl}} = \frac{1}{2}m\omega_M^2 A^2$ in terms of the classical energy scale $E_0 = \frac{1}{2}m\omega_M^2 x_{\text{FWHM}}^2$ as function of driving \mathcal{P} and detuning Δ/ω_M . These are the parameters that can typically be varied in a given experimental setup.

For sufficiently strong driving, self-induced oscillations appear around integer multiples of the cantilever frequency, $\Delta \approx n\omega_M$. For a cavity decay rate $\kappa = 0.5\omega_M$ assumed in Fig. 3, the different bands are distinguishable at lower driving; for larger κ (or for stronger driving), the various ‘sidebands’ merge. For the lower-order sidebands, the nonzero amplitude solution connects continuously to the zero amplitude solution, which becomes unstable. This is an example of a (supercritical) Hopf bifurcation into a limit cycle.

The vertical faces, shown gray in Fig. 3, for $\Delta \approx 2\omega_M$ and $\Delta \approx 3\omega_M$ are connected to the sudden appearance of attractors with a finite amplitude. For example, while approaching the detuning of $\Delta = 2\omega_M$ at fixed \mathcal{P} (the solid line in Fig. 3 refers to $\mathcal{P} = 1.47 \cdot 10^{-3}$), a finite amplitude solution appears, although $A = 0$ remains stable. In Ref. [17] the existence of higher-amplitude stable attractors and, correspondingly, dynamic multistability were discussed.

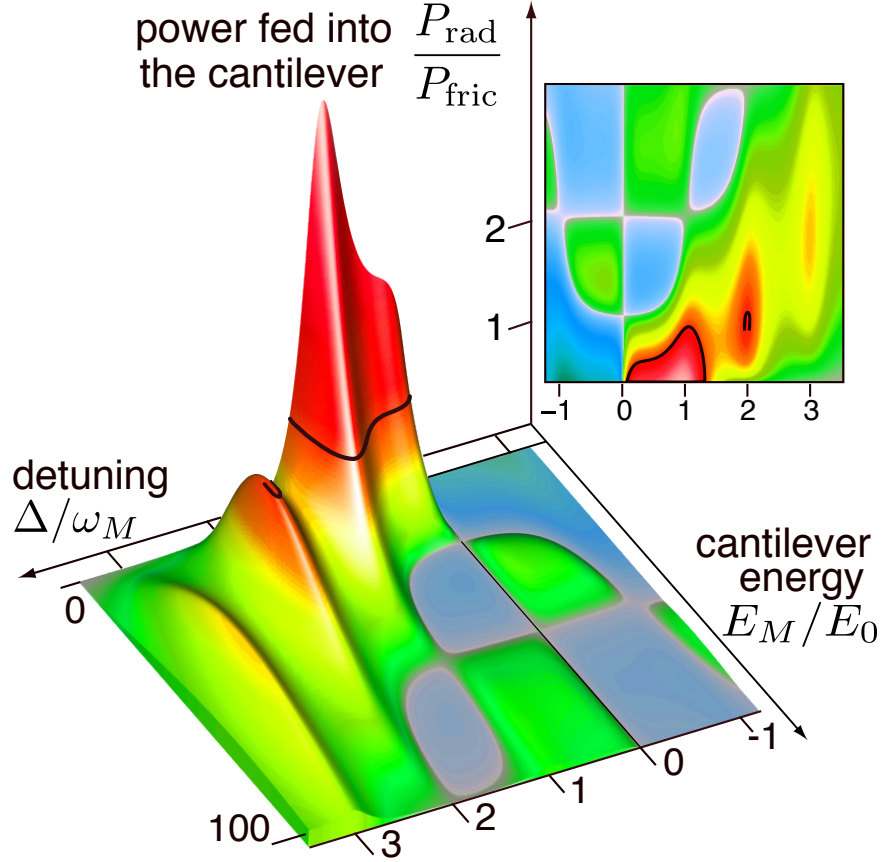


Figure 2: Classical self-induced oscillations of the coupled cavity-cantilever system. The radiation pressure acting on the cantilever provides an average mechanical power input of P_{rad} . The ratio $P_{\text{rad}}/P_{\text{fric}}$ of this power P_{rad} vs. the loss due to mechanical friction, P_{fric} , is shown as a function of the detuning Δ and the cantilever's oscillation energy E_M , at fixed laser input power \mathcal{P} . The oscillation energy $E_M = m\omega_M^2 A^2/2$ is shown in units of E_0 , where $E_M/E_0 = (A/x_{\text{FWHM}})^2$. Self-induced oscillations require $P_{\text{rad}} = P_{\text{fric}}$. This condition is fulfilled along the horizontal cut at $P_{\text{rad}}/P_{\text{fric}} = 1$ (see black line and the inset depicting the same plot, viewed from above). These solutions are stable if the ratio $P_{\text{rad}}/P_{\text{fric}}$ decreases with increasing oscillation amplitude A . The blue regions at the floor of the plot indicate that P_{rad} is negative, resulting in cooling. The cavity decay rate is $\kappa = 0.5\omega_M$, the mechanical damping is chosen as $\Gamma_M/\omega_M = 1.47 \cdot 10^{-3}$, and the input power as $\mathcal{P} = 6.05 \cdot 10^{-3}$; these parameters are also used in figures 3, 4, 5, and 6, and will be referred to as Γ_M^* and \mathcal{P}^* .

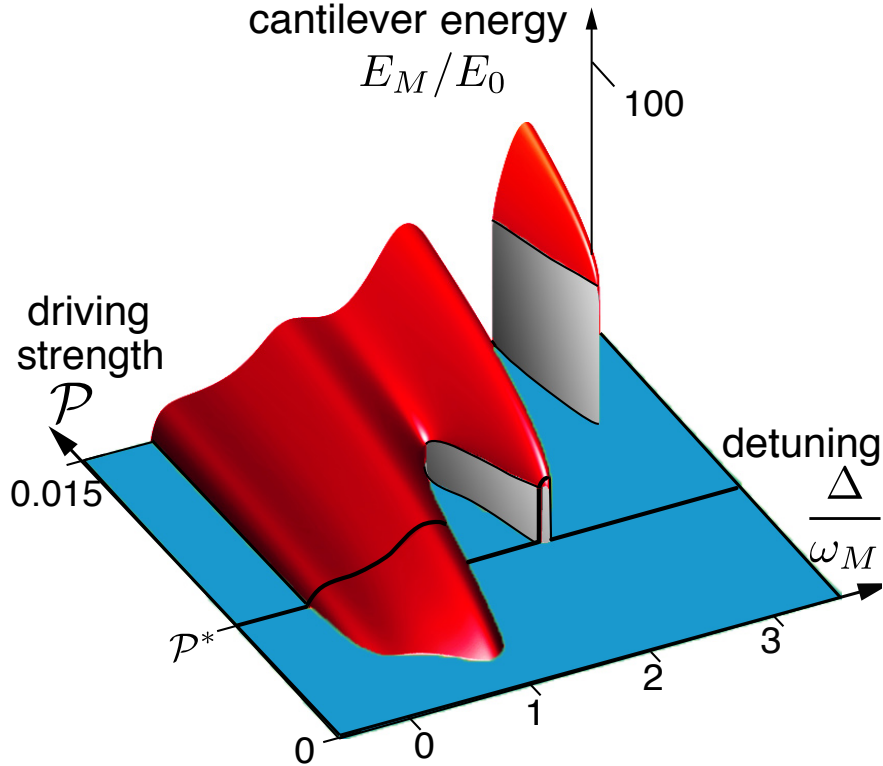


Figure 3: Cantilever oscillation energy $E_M \propto A^2$ versus detuning Δ and laser input power \mathcal{P} . This plot (in contrast to Fig. 2) shows only the stable oscillation amplitude, but as a function of variable input power. The particular value \mathcal{P}^* corresponding to Fig. 2, and the resulting profile of oscillation amplitudes are indicated by a black line. The green floor of the plot indicates regions without self-induced oscillations. The other system parameters are as in Fig. 2. The continuous onset of the self-oscillations in the sidebands at $\Delta/\omega_M = 0, 1$ (which merge for the present parameter values) represents a supercritical Hopf bifurcation, from $A = 0$ to $A \neq 0$. At higher sidebands, an attractor with a finite $A \neq 0$ appears discontinuously, while $A = 0$ remains a stable solution.

3.2 Rate equation approach

Before embarking on a full quantum-mechanical treatment of the coupled cavity-cantilever system, it is instructive to discuss a more simple method to capture some nonclassical effects, in particular the response of the cantilever to the photon shot noise. For that purpose, we consider the shot noise spectrum of the driven cavity, decoupled from the cantilever,

$$S_{FF}(\omega) = \left(\frac{\hbar g}{x_{\text{ZPF}}} \right)^2 S_{nn}(\omega) = \left(\frac{\hbar g}{x_{\text{ZPF}}} \right)^2 \bar{n} \frac{\kappa}{(\omega + \Delta)^2 + (\kappa/2)^2}, \quad (10)$$

where

$$\bar{n} = \frac{\mathcal{P}}{8\zeta^2} \frac{(\omega_M/\kappa)^2}{(\Delta/\omega_M)^2 + (\kappa/2\omega_M)^2} \quad (11)$$

is the mean number of photons in the cavity. The maximum occupation $n_{\max} = \mathcal{P}\omega_M^4/(2\kappa^4\zeta^2) = 4\alpha_L^2/\kappa^2$ occurs at zero detuning. We note that in using the unperturbed, intrinsic shot noise spectrum for an optical cavity in the absence of optomechanical effects, we neglect the modification of that spectrum due to the backaction of the cantilever motion.

The asymmetry of the shot noise spectrum is important for the dynamics of the cantilever. The spectral density of the radiation-pressure force at positive frequency ω_M (negative frequency $-\omega_M$) yields the probability of the cavity absorbing a phonon from (emitting a phonon into) the cantilever [12].

For a red-detuned laser impinging on the cavity ($\Delta < 0$), the cavity's noise spectrum peaks at positive frequencies and the cavity tends to rather absorb energy from the cantilever. As a consequence, the mechanical damping rate for the cantilever is increased, leading to cooling if one starts with a sufficiently hot cantilever. In the opposite Raman-like process taking place at $\Delta > 0$, a blue-detuned laser beam will preferentially lose energy to the cantilever, so that it matches the cavity's resonance frequency. The effective optomechanical damping rate,

$$\Gamma_{\text{opt}} = \zeta^2\kappa^2[S_{nn}(+\omega_M) - S_{nn}(-\omega_M)], \quad (12)$$

is then negative. The corresponding heating of the mechanical cantilever is counteracted by the mechanical damping Γ_M . Simple rate equations for the occupancy of the cantilever yield a thermal distribution for the cantilever phonon occupation number n_M , with [12]

$$\langle \hat{c}^\dagger \hat{c} \rangle = \langle \hat{n}_M \rangle = \frac{\zeta^2\kappa^2 S_{nn}(-\omega_M) + \bar{n}_{\text{th}}\Gamma_M}{\Gamma_{\text{opt}} + \Gamma_M}. \quad (13)$$

The effective temperature, T_{eff} , is related by $\langle \hat{n}_M + 1 \rangle / \langle \hat{n}_M \rangle = \exp[\hbar\omega_M/(k_B T_{\text{eff}})]$ to the mean occupation number. The equilibrium mechanical mode occupation number, \bar{n}_{th} , is determined by the mechanical bath temperature, which is taken as zero in the following. In contrast to first appearance, the mean occupation number of the cantilever given in Eq. (13) does not depend on the quantum parameter ζ , as $\zeta^2 S_{nn}$ is independent of ζ . This is because $S_{nn} \sim \bar{n} \sim 1/\zeta^2$, see Eq. (11). The cantilever energy, therefore, only trivially depends on the quantum parameter as $E_M/E_0 = 4\zeta^2 \langle \hat{n}_M \rangle$, so that it vanishes in the classical limit, where $\zeta^2 \propto \hbar \rightarrow 0$.

In general, the phonon number in Eq. (13) can increase due to two distinct physical effects: On the one hand, the numerator can become larger, due to the influence of photon shot noise impinging on the cantilever, represented by S_{nn} . On the other hand, the denominator can become smaller due to Γ_{opt} becoming negative. In the latter case, the fluctuations acting on the cantilever (both thermal and shot noise) are amplified. This effect is particularly pronounced just below the threshold of instability, where $\Gamma_M + \Gamma_{\text{opt}} = 0$ (see below).

In the resolved sideband limit $\kappa \ll \omega_M$ (at weak driving) the cantilever occupation $\langle \hat{n}_M \rangle$ will peak around zero detuning, where the number of photons in the cavity is large, and around a detuning of $\Delta = \omega_M$. At the latter value of detuning the aforementioned Raman process is maximally efficient as a photon entering the cavity will exactly match the resonance frequency after exciting a phonon in the cantilever. This dependence of cantilever occupation (or the corresponding energy) on the detuning is shown in Fig. 4.

The approach sketched above can be modified slightly to take account of the modification of the cavity length due to a static shift of the cantilever mirror by radiation pressure. Approaching the resonance of the cavity from below, the increasing number of photons inside the cavity will increase the cavity length due to their radiation pressure on the mirror, bringing the system even closer to the resonance. The effect of the static shift of the mirror on the mean occupation of the cavity can be included self-consistently, leading to the tilt of the peak around the resonance, shown by the dash-dotted line in Fig. 4(a). The same figure also includes results of the full quantum mechanical approach, which will be discussed in the next section.

For larger κ , the two peaks in the cantilever excitation merge. Higher-order sidebands are not resolved within this approach, since they would require taking care of the modification of S_{FF} due to the cantilever's motion.

Classical self-induced oscillations occur in a regime of larger driving, where the optomechanical damping rate Γ_{opt} of Eq. (12) becomes negative. They appear once amplification exceeds intrinsic damping, i.e. when $\Gamma_{\text{opt}} + \Gamma_M < 0$. The simple rate equation approach lacks any feedback mechanism to stop the divergence of the phonon number. The classical solution demonstrates how this feedback (i.e. the resulting change in the dynamics of the radiation field) makes the mechanical oscillation amplitude saturate at a finite level. In addition, it shows the onset of self-induced oscillations to occur at a smaller detuning, due to the effective shift of the cantilever position explained above.

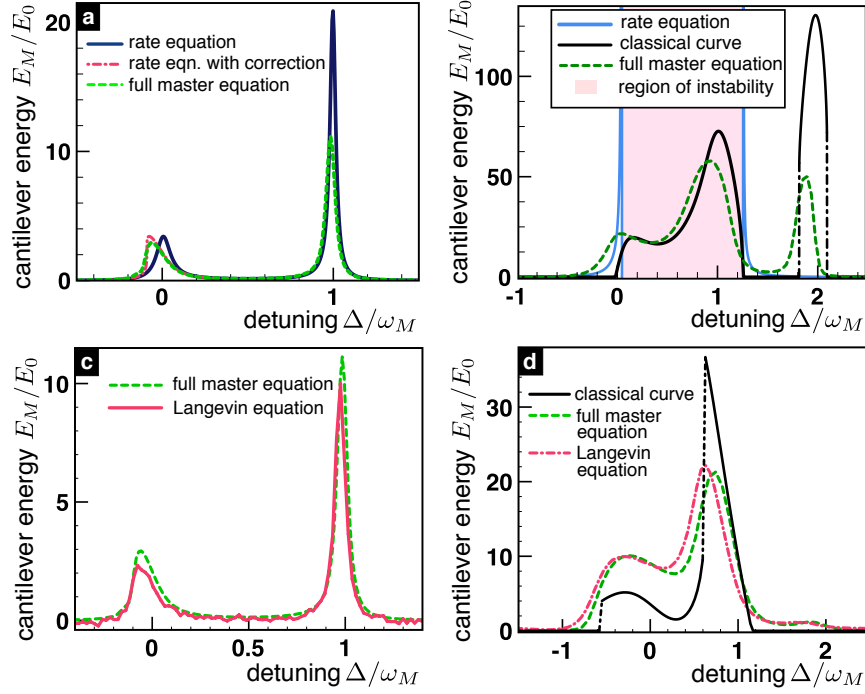


Figure 4: Cantilever energy versus detuning for a cavity driven below [(a),(c)] and above [(b), (d)] the onset of self-induced oscillations. Note $E_M/E_0 = 4\zeta^2 \langle \hat{n}_M \rangle$. (a) Below the onset, the cantilever amplitude would vanish according to the classical analysis that does not incorporate fluctuations. However, the cantilever is susceptible to the photon shot noise (the parameters are $\kappa/\omega_M = 0.1$, $\mathcal{P} = 8.4 \cdot 10^{-3}$, $\Gamma_M/\omega_M = 5 \cdot 10^{-3}$, and $\zeta = 1.0$), leading to finite phonon numbers in the cantilever, particularly around the resonance $\Delta = 0$ and at the first sideband $\Delta = \omega_M$ (see main text). This is captured by the full quantum master equation, as well as (approximately) by the rate equation, whose results improve when taking into account the corrections due to the shift of the cantilever position \bar{x} . (b) For stronger driving, the classical solution yields self-oscillations (the parameters are \mathcal{P}^* , Γ_M^* as in Fig. 3, but $\kappa/\omega_M = 0.3$). The rate equation correctly predicts the onset of the linear instability, but not the nonlinear regime. [The shift in \bar{x} was not taken into account, hence the slight discrepancy vs. the classical solution] The master equation results are shifted to lower detuning and describe sub-threshold amplification and heating as well as self-induced oscillations above threshold, modified and smeared due to quantum effects (as shown for a quantum parameter of $\zeta = x_{\text{ZPF}}/x_{\text{FWHM}} = 1$). (c) Including the zero-point fluctuations in a semiclassical approach via Langevin equations gives results that agree well with both the results from the rate equation and the full master equation, shown here for parameters as in (a). (d) Above the onset of self-induced oscillations the semiclassical approach mimicks results from the quantum master equation partially. The parameters for this plot are $\kappa/\omega_M = 0.3$, $\Gamma_M = 50\Gamma_M^*$, $\mathcal{P} = 20\mathcal{P}^*$, $\zeta = 1$.

In Fig. 4(b) we show results for the detuning dependence of the mean energy of the cantilever obtained from this rate equation approach below the threshold of classical self-induced oscillations. The coupled cavity-cantilever system acts as an amplifier of fluctuations, increasing the occupation of higher number states of the cantilever well before classical oscillations set in. At the onset of classical self-induced oscillations the rate equation result diverges. A full quantum-mechanical treatment describes the crossover of the cantilever dynamics from quantum-fluctuation induced heating to self-induced oscillations as will be discussed now.

3.3 Quantum master equation method

The evolution of the coupled quantum system comprised of the cantilever and the optical cavity is described by the Hamiltonian of Eq. (3). Dissipation arises from the coupling of the mechanical mode to a bath and due to the opening of the cavity to the outside. While the former results in mechanical damping with a rate Γ_M , the latter is associated with the ringdown rate of the cavity κ . In the present paper, we will assume the mechanical bath to be at zero temperature, where quantum effects are most pronounced in steady state. A future, more realistic treatment, should relax this assumption and deal with the nonequilibrium dynamics that results when a mechanical system is first cooled optomechanically and then switched to the unstable side.

The system can be described by a reduced density matrix $\hat{\rho}$ for the mechanical cantilever mode and the optical mode of the cavity. In the frame rotating at the laser frequency, the time evolution of the density matrix $\hat{\rho}$ is given by

$$\frac{d}{dt}\hat{\rho} = \frac{[\hat{H}_0, \hat{\rho}]}{i\hbar} + \Gamma_M \mathcal{D}[\hat{c}] + \kappa \mathcal{D}[\hat{a}], \quad (T \equiv 0) \quad (14)$$

where $\mathcal{D}[\hat{A}] = \hat{A}\hat{\rho}\hat{A}^\dagger - \frac{1}{2}\hat{A}^\dagger\hat{A}\hat{\rho} - \frac{1}{2}\hat{\rho}\hat{A}^\dagger\hat{A}$ denotes the standard Lindblad operator. The Hamilton operator \hat{H}_0 describes the coherent part of the evolution of the coupled cavity-cantilever system,

$$\hat{H} = \hat{H}_0 + \hat{H}_\kappa + \hat{H}_\Gamma.$$

For the numerical evaluation, we rewrite Eq. 14 as $d\hat{\rho}/dt = \mathcal{L}\hat{\rho}$, with a Liouvillian superoperator \mathcal{L} . We then interpret the density matrix as a vector, whose time evolution is governed by the matrix \mathcal{L} . The density matrix at long times (in steady state) is then given by the eigenvector of \mathcal{L} with eigenvalue 0. The numerical calculation of this eigenvector is much more efficient than a simulation of the full time evolution. Since we are dealing with large sparse matrices, it is convenient to employ an Arnoldi method that finds a few eigenvalues and eigenvectors of \mathcal{L} by iterative projection. For Hermitean matrices, the Arnoldi method is also known as the Lanczos algorithm.

In practice, the numerical approach used here sets strong limits on the dimension of the Hilbert space. We need to take into account the N_a lowest Fock states of the cavity and the N_c lowest Fock states of the mechanical cantilever,

resulting in a Liouvillian superoperator with $(N_a \times N_c)^4$ elements. This puts more severe restrictions on our treatment of the coupled cavity-cantilever system than encountered in similar treatments of comparable systems. For example, nanoelectromechanical systems, where an oscillator is coupled to a normal-state or superconducting single-electron transistor (SET), will have to account for only a very limited number of charge states of the SET (namely those few involved in the relevant transport cycle). As a consequence, a larger number of Fock states can be included, e.g., 70 number states of the oscillator were kept in Ref. [28]. In some cases it was furthermore considered sufficient to treat only the incoherent dynamics of the mechanical oscillator, i.e., only the elements of the density matrix diagonal in the oscillator's Fock space, thereby reaching 200 number states of a mechanical mode coupled to a normal-state SET [41]. The restricted number of Fock states that can be considered here makes it more difficult to fully bridge the gulf to the classical regime of motion of the mechanical cantilever. [(N_a, N_c) = (8,16) for Fig. 4(a),(c),(d), (4,22) for Figs. 4(b), 5 and for the first two panels of 6, (3,35) for the last panel of Fig. 6]

A first comparison of results of the quantum master equation to the classical solution and the results of the rate equation was already shown in Fig. 4. We find that the full quantum results do not qualitatively differ from the rate equation results provided the parameters are chosen sufficiently far from the onset of self-induced oscillations. However, only the quantum master equation approach is able to describe the crossover from sub-threshold quantum fluctuations (where $E_M \propto \zeta^2$) to the large classical cantilever energies associated with self-induced oscillations.

In Fig. 5 we demonstrate the influence of the quantum parameter $\zeta = x_{\text{ZPF}}/x_{\text{FWHM}}$ governing the crossover between the classical and the quantum regime.

Figure 5(a) shows the cavity photon number, normalized to its value at resonance, n_{max} . For our choice of driving parameter \mathcal{P} , the maximal occupation n_{max} is low, so that a small number of Fock states suffices for describing the cavity in the quantum master equation. This allows to account for enough number states of the cantilever to reach the regime of self-induced oscillations. The classical solution (solid black line) consists of the broad Lorentzian of the isolated cavity, on top of which additional peaks appear. These are due to the classical self-induced oscillations occurring at the sidebands $\Delta = \omega_M, 2\omega_M, \dots$ in the coupled cavity-cantilever system. Figure 5(c) displays the cantilever energy E_M/E_0 as a function of the detuning, Δ/ω_M , with features that parallel those found for the photon number. The classical curve in (b), shown in black, corresponds to the cut indicated by the solid line in Fig. 3. For the chosen driving power, the second sideband at $\Delta = \omega_M$ just starts to appear, while the first sideband is merged with the resonance at $\Delta = 0$, which shows up as a slight shoulder. The sharpness and strength of these features also depend on the values of mechanical damping and cavity decay rate. Results of our solution of the quantum master equation are shown for three different values of the quantum parameter $\zeta = x_{\text{ZPF}}/x_{\text{FWHM}}$. Due to restrictions of the numerical resources, it was not feasible to map out a wider range of values of the parameter ζ , although the

range analysed here already suffices to describe the quantum-classical crossover.

The quantum master equation shows results that are qualitatively similar to the classical solution in the regime of self-induced oscillations, with the peaks being progressively broadened, reduced in height, and shifted to lower detuning for increasing values of the quantum parameter ζ . Numerical evidence indicates that quantum correlations between the cantilever position operator \hat{x} and the photon operators \hat{a}^\dagger, \hat{a} may cause the observed shift. As expected, the discrepancy between the quantum mechanical and the classical result reduces with diminishing quantum parameter ζ . In Fig. 5(b), we show the dependence of the cantilever energy on the quantum parameter, for two different values of the detuning. In the sub-threshold regime of amplification/heating the cantilever energy scales as ζ^2 , as discussed above. In any case, the classical limit is clearly reached as $\zeta \rightarrow 0$.

At the second sideband a classical solution of finite amplitude coexists with a stable zero-amplitude solution (compare Fig. 2 and last panel of Fig. 6). The black curve in Fig. 5(b), showing the finite amplitude solution, may therefore deviate substantially from the $\hbar \rightarrow 0$ limit of the quantum mechanical result. In general, the average value of E_M , shown here, will be determined by the relative weight of the two solutions (which are connected by tunneling due to fluctuations), as well as fluctuations of E_M for each of those two attractors.

3.4 Langevin equation

To get an estimate of the influence of quantum fluctuations, we compare the results of the quantum master equation to numerical simulations of classical Langevin equations that try to mimick the quantum noise. The resulting description of the quantum-to-semiclassical crossover is illustrated in Figs. 4(c). To imitate both the zero-point fluctuations of the mechanical oscillator and the shot-noise inside the cavity, we add white noise terms to Eqs.4 and 5:

$$\dot{\alpha} = [i(\Delta + g \frac{x}{x_{\text{ZPF}}}) - \frac{\kappa}{2}] \alpha - i\alpha_L + \sqrt{\kappa/2} \alpha_{in} \quad (15)$$

$$\ddot{x} = -\omega_M^2 x + \frac{\hbar g}{m x_{\text{ZPF}}} |\alpha|^2 - \Gamma_M \dot{x} + \sqrt{\hbar \omega_M \Gamma / m} \xi, \quad (16)$$

where $\langle \alpha_{in} \rangle = \langle \xi \rangle = 0$ and $\langle \alpha_{in}(t) \alpha_{in}^*(t') \rangle = \langle \xi(t) \xi(t') \rangle = \delta(t - t')$. The coefficients in front of the noise terms are chosen such that in the absence of optomechanical coupling we obtain the zero-point fluctuations, i.e. $\langle |\alpha|^2 \rangle = 0.5$ away from resonance and $\frac{m \omega_M^2}{2} \langle x^2 \rangle = \frac{\hbar \omega_M}{4}$. The mean zero-point energy of the cantilever is subtracted from the curve in Fig.4(c).

For parameters below the onset of self-sustained oscillations, this semiclassical approach leads to good qualitative agreement with the quantum mechanical description, as can be seen in Fig. 4(c) for parameters that are the same as those of 4(a). Still, the Langevin approach can mimick the results from the master equation only partially. In particular, the approximation gets worse

when dealing with low photon numbers. This is because the Langevin equation introduces artificial fluctuations of the radiation pressure force in the vacuum state. Indeed, $|\alpha|^2$ has a finite variance even in the ground state of the photon field, in contrast to $\hat{a}^\dagger \hat{a}$.

3.5 Wigner density and phonon number distribution

In figure 6, we go beyond the average cantilever phonon number and present results both for the phonon number probability distribution, as well as the full Wigner density of the cantilever, defined as

$$W(x, p) = \frac{1}{\pi\hbar} \int_{-\infty}^{+\infty} \langle x - y | \hat{\rho} | x + y \rangle e^{2ipy/\hbar} dy. \quad (17)$$

This figure demonstrates the different nature of the cantilever dynamics in the sub-threshold regime and above threshold, where self-induced oscillations occur. Below the threshold (for a detuning $\Delta_a = -0.45\omega_M$ as indicated in Fig. 5, quantum parameter $\zeta = 1$, and other parameters as in Fig. 5) the occupation of the cantilever is thermal, with an effective temperature determined by the effective optomechanical and mechanical damping rates, cf. Eq. (13). Consequently, the Wigner density shows a broad peak around the origin of the $x - p$ plane of cantilever position and momentum (the static shift of the cantilever due to the radiation pressure is very small). For a detuning of $\Delta_b = -0.2\omega_M$, self-induced oscillations occur. The probability distribution for the phonon number shows some thermal broadening, but an additional peak appears at a finite phonon number. In the Wigner density plot this results in a crater-like feature, which corresponds to a mixture of coherent states with essentially fixed amplitude but arbitrary phases. This captures the fact that the phase of the self-induced oscillations is completely arbitrary also in the classical solution. The energy corresponding to the phonon number at which the distribution peaks, compares fairly well to the oscillation energy obtained from the classical solution. Only the shift towards lower values of detuning as shown in Fig. 5(b) puts restrictions on a detailed quantitative comparison.

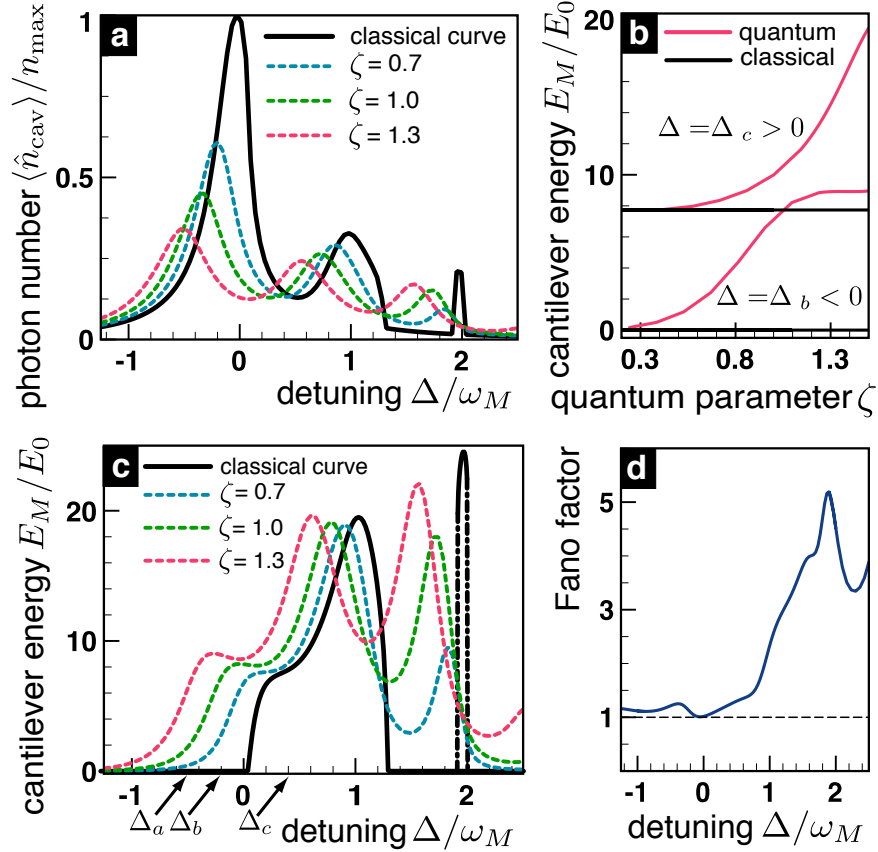


Figure 5: Comparison of classical and quantum results. (a) Number of photons inside the cavity as a function of detuning, and (c) energy of the cantilever versus detuning for Γ_M^* , \mathcal{P}^* and $\kappa/\omega_M = 0.5$. The dotted curves show results from the quantum master equation for different values of the quantum parameter $\zeta = 1.3$ (pink), $\zeta = 1.0$ (green) and $\zeta = 0.7$ (blue), which are compared with the solution of the classical equations of motion (black solid curve). As $\zeta \rightarrow 0$, the quantum result approaches the classical curve. See main text for a detailed discussion. (b) The energy of the cantilever as a function of the quantum parameter ζ for fixed detunings $\Delta_b/\omega_M = -0.2$ and $\Delta_c/\omega_M = 0.4$ (the detuning value Δ_a indicated in (b) is used in Fig. 6). (d) Fano factor $(\langle \hat{n}_M^2 \rangle - \langle \hat{n}_M \rangle^2) / \langle \hat{n}_M \rangle$ vs. detuning, for $\zeta = 1$. For a coherent state whose occupation number follows a Poisson distribution, the Fano factor is 1 (dashed black line). Close to the resonance (and far away from it, where $\langle \hat{n}_M \rangle = 0$), the results of the quantum master equation approach this value. The Fano factor becomes particularly large near the second sideband, where we observe coexistence of different oscillation amplitudes (see Fig. 6).

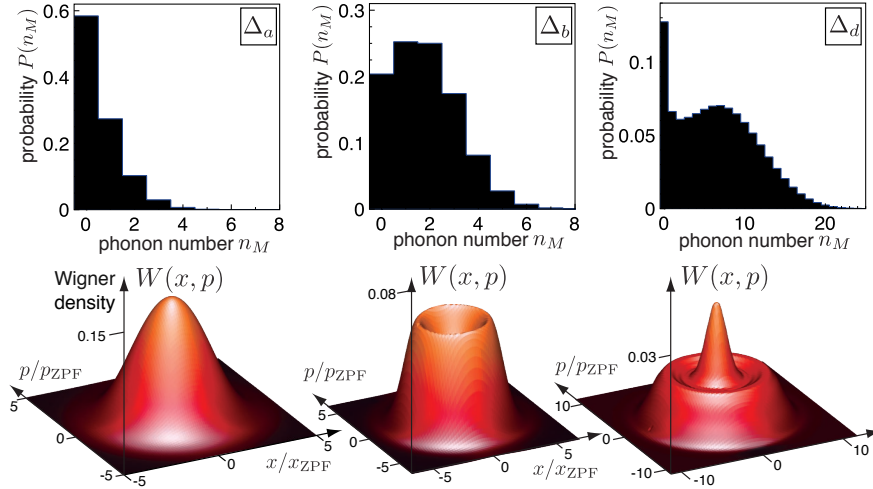


Figure 6: Distribution functions $P(n_M)$ of the cantilever occupation and Wigner functions $W(x, p)$ [rescaled by $x_{\text{ZPF}}p_{\text{ZPF}}$] of the cantilever for $\Delta_a = -0.45\omega_M$, $\Delta_b = -0.2\omega_M$, $\Delta_d = 1.72\omega_M$ [corresponding to the detuning values also indicated in Fig. 5(b); further parameters as in Fig. 5 with $\zeta = 1.0$; for Δ_d the mechanical damping rate is reduced to $\Gamma_M/\omega_M = 1.2 \cdot 10^{-3}$]. Below the threshold of self-induced oscillations, a broadened distribution is found corresponding to an increased effective temperature, cf. Eq. (13) (left panels, Δ_a); self-induced oscillations are visible as a finite amplitude ring in the middle and the right panel. Dynamical multistability (i.e. co-existence of several attractors) in the classical solution becomes apparent both in the distribution and the Wigner density, where a double-peaked structure develops.

For a value of the detuning located in the second sideband, $\Delta_d = 1.72\omega_M$, we find a probability distribution with a peak for the occupation of the cantilever ground state, and a broader peak at a finite occupation number (mechanical damping is slightly decreased to display more pronounced features). Likewise, the Wigner density consists of a sharp peak at the origin, surrounded by a broader ring representing finite amplitude oscillations. This corresponds to the existence of two stable attractors in the classical analysis, with vanishing and finite oscillation amplitude, respectively. Similar results for the Wigner densities were found in Ref. [28] for a cantilever driven by a superconducting single-electron transistor.

4 Conclusion

We presented a fully quantum mechanical treatment of a driven optical cavity coupled to a mechanical cantilever by radiation pressure. Light-induced forces can yield a negative contribution to the damping of the cantilever, causing

amplification of fluctuations and even instabilities of the cantilever dynamics.

In the present paper we first reviewed briefly the classical solution and discussed the existence of self-induced oscillations and the resulting attractor diagram of the system. We paid particular attention to the resolved-sideband regime $\kappa \ll \omega_M$, which is now increasingly studied in experimental setups. Here the instabilities clearly occur at sidebands, where the detuning matches an integer multiple of the mechanical frequency.

Within a simple rate equation approach, we were able to discuss the influence of the photon shot noise and quantum fluctuations well below the instability threshold. The full quantum-mechanical treatment, based on a numerical solution of the quantum master equation, is able to completely describe both regimes (below and above threshold). It has been complemented by numerical studies of a Langevin equation that includes the zero-point fluctuations in a semiclassical way. We studied the crossover between the quantum and classical regime, which is governed by the quantum parameter, $\zeta = x_{\text{ZPF}}/x_{\text{FWHM}}$, denoting the ratio between the mechanical zero-point fluctuation amplitude and the width of the optical resonance. Signatures of the self-induced oscillations are also found in the full quantum mechanical solution, even at larger values of ζ . In regions of dynamical multistability, the different attractors show up simultaneously in the steady state of the cantilever, since the quantum noise can induce transitions between those attractors. Finally, we characterized the mechanical motion in the various regimes by discussing the phonon number probability distribution as well as the Wigner density.

Acknowledgments

We thank A. Clerk, S. Girvin, K. Karrai, C. Neuenhahn, C. Metzger, I. Favero, D. Rodrigues, and J. Harris for discussions and fruitful collaboration on the optomechanical instability. We acknowledge support by the DFG, in the form of the Nanosystems Initiative Munich (NIM), the SFB 631, and the Emmy-Noether program.

References

- [1] V.B. Braginsky and A.B. Manukin. Ponderomotive effects of electromagnetic radiation. *Soviet Physics JETP*, 25:653, 1967.
- [2] V. B. Braginsky, A. B. Manukin, and M. Yu. Tikhonov. Investigation of dissipative ponderomotive effects of electromagnetic radiation. *Soviet Physics JETP*, 31:829, 1970.
- [3] A. Dorsel, J. D. McCullen, P. Meystre, E. Vignes, and H. Walther. Optical bistability and mirror confinement induced by radiation pressure. *Phys. Rev. Lett.*, 51:1550, 1983.

- [4] P. F. Cohadon, A. Heidmann, and M. Pinard. Cooling of a mirror by radiation pressure. *Phys. Rev. Lett.*, 83:3174, 1999.
- [5] C. Höhberger-Metzger and K. Karrai. Cavity cooling of a microlever. *Nature*, 432:1002, 2004.
- [6] O. Arcizet, P. F. Cohadon, T. Briant, M. Pinard, and A. Heidmann. Radiation-pressure cooling and optomechanical instability of a micro-mirror. *Nature*, 444:71, 2006.
- [7] S. Gigan et al. Self-cooling of a micromirror by radiation pressure. *Nature*, 444:67, 2006.
- [8] A. Schliesser, P. Del’Haye, N. Nooshi, K. J. Vahala, and T. J. Kippenberg. Cooling of a micro-mechanical oscillator using radiation pressure induced dynamical back-action. *Phys. Rev. Lett.*, 97:243905, 2006.
- [9] D. Kleckner and D. Bouwmeester. Sub-kelvin optical cooling of a micromechanical resonator. *Nature*, 444:75, 2006.
- [10] T. Corbitt et al. Toward achieving the quantum ground state of a gram-scale mirror oscillator. *Phys. Rev. Lett.*, 98:150802, 2007.
- [11] J. D. Thompson, B. M. Zwickl, A. M. Jayich, F. Marquardt, S. M. Girvin, and J. G. E. Harris. Strong dispersive coupling of a high finesse cavity to a micromechanical membrane. *arXiv:0707.1724*, 2007.
- [12] F. Marquardt, J. P. Chen, A. A. Clerk, and S. M. Girvin. Quantum theory of cavity-assisted sideband cooling of mechanical motion. *Phys. Rev. Lett.*, 99:093902, 2007.
- [13] I. Wilson-Rae, N. Nooshi, W. Zwerger, and T. J. Kippenberg. Theory of ground state cooling of a mechanical oscillator using dynamical back-action. *Phys. Rev. Lett.*, 99:093901, 2007.
- [14] J. M. Aguirregabiria and L. Bel. Delay-induced instability in a pendular Fabry-Perot cavity. *Phys. Rev. A*, 36:3768, 1987.
- [15] C. Fabre, M. Pinard, S. Bourzeix, A. Heidmann, E. Giacobino, and S. Reynaud. Quantum-noise reduction using a cavity with a movable mirror. *Phys. Rev. A*, 49:1337, 1994.
- [16] V. B. Braginsky, S. E. Strigin, and S. P. Vyatchanin. Parametric oscillatory instability in Fabry-Perot interferometer. *Physics Letters A*, 287:331, 2001.
- [17] F. Marquardt, J. G. E. Harris, and S. M. Girvin. Dynamical multistability induced by radiation pressure in high-finesse micromechanical optical cavities. *Phys. Rev. Lett.*, 96:103901, 2006.

- [18] C. Hühberger and K. Karrai. Self-oscillation of micromechanical resonators. *Nanotechnology 2004, Proceedings of the 4th IEEE conference on nanotechnology*, page 419, 2004.
- [19] T. Carmon, H. Rokhsari, L. Yang, T. J. Kippenberg, and K. J. Vahala. Temporal behavior of radiation-pressure-induced vibrations of an optical microcavity phonon mode. *Phys. Rev. Lett.*, 94:223902, 2005.
- [20] T. J. Kippenberg, H. Rokhsari, T. Carmon, A. Scherer, and K. J. Vahala. Analysis of radiation-pressure induced mechanical oscillation of an optical microcavity. *Phys. Rev. Lett.*, 95:033901, 2005.
- [21] M. Ludwig, C. Neuenhahn, C. Metzger, A. Ortlieb, I. Favero, K. Karrai, and F. Marquardt. Self-induced oscillations in an optomechanical system. *arXiv:0711.2661*, 2007.
- [22] K. R. Brown, J. Britton, R. J. Epstein, J. Chiaverini, D. Leibfried, and D. J. Wineland. Passive cooling of a micromechanical oscillator with a resonant electric circuit. *Phys. Rev. Lett.*, 99:137205, 2007.
- [23] Ya. M. Blanter, O. Usmani, and Yu. V. Nazarov. Single-electron tunneling with strong mechanical feedback. *Phys. Rev. Lett.*, 93(13):136802, Sep 2004.
- [24] A. A. Clerk and S. Bennett. Quantum nanoelectromechanics with electrons, quasi-particles and Cooper pairs: effective bath descriptions and strong feedback effects. *New Journal of Physics*, 7:238, 2005.
- [25] M. P. Blencowe, J. Imbers, and A. D. Armour. Dynamics of a nanomechanical resonator coupled to a superconducting single-electron transistor. *New Journal of Physics*, 7:236, 2005.
- [26] A. Naik et al. Cooling a nanomechanical resonator with quantum back-action. *Nature*, 443:193, 2006.
- [27] S. D. Bennett and A. A. Clerk. Laser-like instabilities in quantum nanoelectromechanical systems. *Phys. Rev. B*, 74:201301, 2006.
- [28] D. A. Rodrigues, J. Imbers, and A. D. Armour. Quantum dynamics of a resonator driven by a superconducting single-electron transistor: a solid-state analogue of the micromaser. *Phys. Rev. Lett.*, 98:067204, 2007.
- [29] D. A. Rodrigues, J. Imbers, T. J. Harvey, and A. D. Armour. Dynamical instabilities of a resonator driven by a superconducting single-electron transistor. *New Journal of Physics*, 9:84, 2007.
- [30] C. A. Regal, J. D. Teufel, and K. W. Lehnert. Measuring nanomechanical motion with a microwave cavity interferometer, 2008.
- [31] D. Meiser and P. Meystre. Coupled dynamics of atoms and radiation-pressure-driven interferometers. *Phys. Rev. A*, 73:033417, 2006.

- [32] K. W. Murch, K. L. Moore, S. Gupta, and D. M. Stamper-Kurn. Measurement of Intracavity Quantum Fluctuations of Light Using an Atomic Fluctuation Bolometer. *arXiv:0706.1005v2*, 2007.
- [33] S. Bose, K. Jacobs, and P. L. Knight. Scheme to probe the decoherence of a macroscopic object. *Phys. Rev. A*, 59:3204, 1999.
- [34] W. Marshall, C. Simon, R. Penrose, and D. Bouwmeester. Towards quantum superpositions of a mirror. *Physical Review Letters*, 91(13):130401, 2003.
- [35] M. Pinard, A. Dantan, D. Vitali, O. Arcizet, T. Briant, and A. Heidmann. Entangling movable mirrors in a double-cavity system. *Europhysics Letters*, 72:747, 2005.
- [36] E. Buks, E. Segev, S. Zaitsev, B. Abdo, and M. P. Blencowe. Quantum nondemolition measurement of discrete fock states of a nanomechanical resonator. *EPL (Europhysics Letters)*, 81(1):10001 (5pp), 2008.
- [37] T. J. Kippenberg and K. J. Vahala. Cavity opto-mechanics. *Optics Express*, 15:17172, 2007.
- [38] F. Marquardt, A. A. Clerk, and S. M. Girvin. Quantum theory of optomechanical cooling. *arXiv:0803.1164 (to be submitted to the proceedings of the "Physics of Quantum Electronics 2008" conference)*, 2008.
- [39] O. Usmani, Ya. M. Blanter, and Yu. V. Nazarov. Strong feedback and current noise in nanoelectromechanical systems. *Physical Review B (Condensed Matter and Materials Physics)*, 75(19):195312, 2007.
- [40] A. Schliesser, R. Riviere, G. Anetsberger, O. Arcizet, and T. J. Kippenberg. Resolved sideband cooling of a micromechanical oscillator. *arXiv:0709.4036*, 2007.
- [41] M. Merlo, F. Haupt, F. Cavaliere, and M. Sasseti. Sub-poissonian phononic population in a nanoelectromechanical system. *New Journal of Physics*, 10(2):023008 (12pp), 2008.